# Assessment of a Novel Toughening Procedure for Composite Vacuum Infusion In-Field Repairs

D. Tzetzis[1], P.J. Hogg[1] and M.Jogia[2]

[1]Queen Mary College, University of London, Department of Materials, London E1 4NS,UK
[2]QinetiQ, Structural Materials Centre, Farnborough, Hampshire GU14 0LX,UK

## ABSTRACT

The present paper is an attempt to highlight the use of the vacuum infusion process as an alternative reliable bonded in-field repair approach. The use of low viscosity (unmodified) epoxy resins for fast infusion rates act both as the consolidation agent of the reinforcement and as the bonding medium on the parent substrate. The major drawback from the processed patch is the brittle behaviour of the infused bondline. The study illustrates that incorporation of polyester and carbon fibres within the infused bondline in the form of veils establish a measure of control over the intermittent crack propagation and increase dramatically the fracture energy in the mode I loading condition. The vacuum infusion repair technology along with the proposed bondline toughening approach is evaluated on a damaged edge-stiffened monolithic CFRP skin for a compression-loading regime. The experimental results suggest that the vacuum infused patch is capable of restoring a surplus of 0.4% failure strain, which is the design limit for primary aerospace composite components.

## 1. INTRODUCTION

The use of carbon fibre-reinforced polymer composite materials in military aircraft is steadily increasing for reasons that are well understood and widely reported. However, the susceptibility of these materials to impact damage ranging from tool drop to ballistic penetration is a growing area of concern. The effects from a potential impact may include delamination and matrix cracking extending well beyond the impact site that may further introduce ingress of contaminants into the structure. In order to restore the desired levels of structural strength and stiffness currently two routes exist. One way is immediate component replacement, if factors such as time, availability and economics can be overcome, ensuring continuation and safe working capability of the structure. The other more time saving and economically viable option is to perform a repair, which additionally, according to current ecological requirements can become a major step for the enhanced product life of the non-recyclable CFRP materials.

The repair of aircraft components by the use of composite patches has been extensively studied over the past 15-20 years [1-6]. Some studies dealt with the repairability of real aircraft structures [1-3] while others have investigated the mechanical behaviour of generic repaired composite panels [4-6]. The technique for repairing the composite components involves removal of the damaged region and re-consolidation of the composite using preferably the same carbon prepreg material bonded with a toughened adhesive film ensuring effective load transfer between the parent structure and repair patch.

The application of bonded composite patches is restricted to repair aircrafts at maintenance bases where the necessary skills and facilities are available to cure the prepreg resin matrices and adhesive films (stored in freezers) and therefore, achieve good quality adhesive bonds. On the other hand, in-field repairs, especially for military aircrafts require an in-situ feasible process in the shortest time span with minimum equipment and materials that can be stored in ambient temperatures. It is important to note that it is very hard to find bonded repair studies to in-field use.

The current accepted in-field method of repairing significant damage in a composite structure is to apply a mechanically-fastened patch because less skill and fewer tools are required. However, this suffers from significant drawbacks such as increase in weight, disruption of airflow and it is difficult if not impossible to be applied to contoured regions. It becomes increasingly important therefore to devise methods that allow bonded composite patches to be transferred from the maintenance base to the field-level. Hand lay- up patches are avoided since they result in inconsistent repair, low volume fractions and high percentage of voids within the bondline that lead to low load carrying capabilities and eventually pop-off of the patch itself [7].

Vacuum infusion is considered to be one of the quickest manufacturing routes to high quality composite product and is expected to gain an increased share of the market for general composites processing [8]. It also provides the flexibility needed for in-field repair in terms of the equipment and materials required. It is relatively easy to perform in reasonable times scales that are appropriate for military aircraft in combat time conditions. The major drawback of the technique is that it needs low viscosity resin systems to achieve fast infusion times. This restricts the inclusion of toughening additives in the resin formulation and can result in brittle bonds susceptible to crack propagation from minor bondline defects that lead to catastrophic failure.

The present paper illustrates a toughening procedure for the bondline of the vacuum infused patch and evaluates the feasibility of the repair process itself becoming a reliable and simple manual in-field repair method. Toughening comes in the form of a discontinuous phase such as polyester and carbon veils positioned along the bondline and co-infused with the patch reinforcement plies. Double Cantilever Beam (DCB) specimens were produced simulating the infusion repair that allowed an assessment of the work of fracture in mode-I. The feasibility of the vacuum infusion repair patch technology coupled with the proposed toughening system is assessed on a monolithic honeycomb edge stiffened carbon skin taken from an aircraft. The compressive performance of the repaired component was compared by testing an identical undamaged component under the same conditions.

## 2. TOUGHENING APPROACH OF INFUSED BONDLINE

### 2.1 Materials and DCB Repair Preparation

Double Cantilever Beam (DCB) test pieces were manufactured to determine the work of fracture of vacuum infused repairs. On pre-fabricated plates, having stacking sequence of $(0,-45{+}45,90)_s$ and representing the parent component, eight plies of carbon T300 carbon 5HS woven fabric were vacuum infused on top with Araldite LY5052 epoxy resin representing the repair patch. The LY5052 resin system was mixed prior to infusion with HY5052 hardener, 63% to 37% by weight respectively. The resin was degassed for 15minutes under full vacuum at 40ºC to further reduce its viscosity for faster infusion. The cure cycle selected after infusion was to heat up the patch to 90°C at 2°C/ min, followed by three hours under the heater mat. After infusion and cure the patches were allowed to cool down to ambient temperature, before debagging.

The surface of the parent component was grit blasted for all the repairs studied using a grit mesh of #30/40 and degreased thoroughly with acetone prior to infusion. Some DCB specimens were manufactured by infusing the woven repair fabric plies directly onto the treated surface denoted as repairs without bondline reinforcement, while for the other DCB specimens, polyester veils and/or carbon veils (fibres running at random orientations) were positioned between the treated surface and the repair woven plies. Fig. 1 shows optical micrographs of the veils used. Three configurations were assessed. One with an intermediate carbon veil of 10 g/m$^2$, one with a polyester veil of 25g/m$^2$ and one with a combination of two layers of polyester veil and in-between a carbon veil (70% polyester fibres and 30% carbon fibres) making a total of three layer configuration. The selection of the veils was based as much for their ready availability as for their prospective performance.

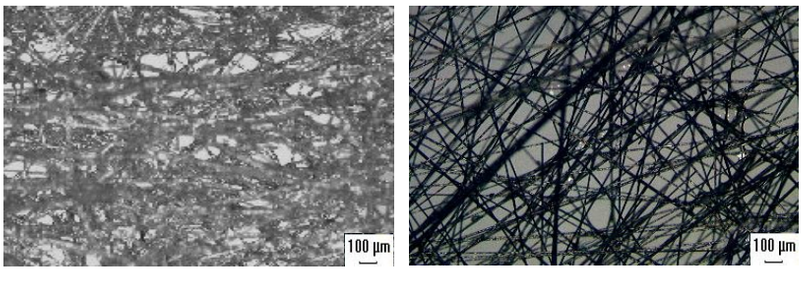


**Fig. 1.** Optical micrographs of a polyester and a carbon veil used as the toughening phase of the infused bondline

The dimensions of the DCB specimens were 120mm x 20mm x 3.6mm and a 12μm thick release film was inserted prior the infusion process to define a 50mm starter crack. The specimen edges just ahead of the insert were coated with a layer of white correction fluid to facilitate crack detection. The specimens were marked from the insert with thin vertical lines every 1mm up to 10mm. The remaining 30mm were then marked every 5mm. The small increments were used to ensure the detection of the crack front after an unstable crack growth in some of the specimens.

2.2. Testing Procedure and Calculation of the Strain Energy Release Rate

The DCB repairs were loaded on an 1122 Instron testing machine equipped with a 1KN load cell by clamping the hinges (pre-bonded on the specimen edges) in the grips. The cross-head speed was 0.5mm/min for the first 10mm of the crack propagation and then was increased to 1mm/min to avoid a very long testing time. Load and displacement were recorded during the tests as the crack propagated, while observations of the crack length at the edge of the specimens were enhanced with a high magnification digital camera.
Various methods are used in the open literature [9] for the calculation of the critical strain energy release rate from the load-displacement and crack length data accumulation, however the compliance calibration method is more suitable for cantilever arms of dissimilar thickness. The compliance calibration approach assumes that the compliance, C, is proportional to $a^n$ and is based on the work of Griffith which states that the driving force for crack growth is that the stored elastic strain energy released when the crack grows must be at least as great as the energy required to create the new surfaces. Assuming linear elastic behaviour the following expression can be derived for the strain energy release rate G in a plate with a through thickness crack.

$$G = \frac{P^2}{2b}\frac{dC}{da} \tag{1}$$

where P is the applied load, b the specimen width, a the crack length and C the sample compliance, which is defined by:

$$C = \frac{\delta}{P} \tag{2}$$

where δ is the displacement. The compliance calibration method as mentioned above uses a plot of compliance C against a crack length a, on a log-log chart. A straight line fit to this curves gives:

$$C = Ka^n \tag{3}$$

where n is the slope of the curve and K is the intercept. At failure by substituting Eq. (2) and Eq. (3) to Eq. (1) the fracture energy $G_{IC}$ is obtained:

$$G_{IC} = \frac{nP_C\delta}{2ba} \tag{4}$$

The initiation of crack growth is difficult to observe and in any case it is highly operator dependent. Therefore, the initiation strain energy release rate was calculated at the point where the load-displacement curve during testing deviated from linearity. This type of calculation assumes that the crack begins to grow from the centre of the insert, within the bondline. The integrity of each bondline under comparison was evaluated from the qualitative and quantitative analysis of the DCB tests. The values of strain energy release rate, $G_I$, calculated gave a quantitative measure of the energy dissipation required to fracture the bondline produced by the vacuum infusion repair process. Post-failure analysis and examination of the fractured surfaces showed qualitatively the mode of failure indicating a

cohesive or adhesion (interfacial) type of failure and hence enabling a judgment as to whether the bondline was capable of resisting to crack initiation and propagation.

## 2.3. Strain Energy Release Rate

Table 1 shows the critical energy release rate values for the DCB tests while Fig. 2 illustrates typical resistance curves (R-curves) obtained from each type of repair. The results obtained for bonds made without the reinforcing veils reveal a rather weak crack R-curve effect, such that the average of the propagation values, being 0.163kJ/m$^2$, did not differ considerably from the initiation value (0.133kJ/m$^2$) indicating that as the crack length was increased low energy was required to continue fracturing the surface.

**Table 1.** Strain energy release rate results from the mode I testing of DCB repairs

| Repair Bondline Condition | $G_{I\text{-}INITIATION}$ (kJ/m$^2$) | Standard Deviation | $G_{I\text{-}PROPAGATION}$ (kJ/m$^2$) | Standard Deviation |
|---|---|---|---|---|
| Without Reinforcement | 0.133 | 0.014 | 0.163 | 0.023 |
| Carbon Fibre Reinforced | 0.421 | 0.064 | 0.474 | 0.082 |
| Polyester Fibre Reinforced | 0.562 | 0.050 | 1.389 | 0.078 |
| Carbon/Polyester Fibre Reinforced | 0.928 | 0.107 | 1.929 | 0.98 |

DCB repairs reinforced with the carbon veil exhibited much higher initiation (0.421kJ/m$^2$) and propagation fracture energy (0.474kJ/m$^2$) values again with small differences between them. At the propagation region there was a clear stick-slip behaviour revealing a rather brittle fracture as expected from the use of the carbon veil. The higher initiation fracture energy compared to DCB repairs without veil was believed to be primarily due to cohesive bondline fracture associated with the infused epoxy resin. This is in contrast to the interfacial fracture related to the Hercules 3501.6 surface resin of the parent prepreg laminate for the repairs without bondline reinforcement. One possibility is that the mechanism of cracking within the infused bondline was linked to the random distribution of the carbon fibres themselves promoting failure at their interface. However, the most probable explanation of the higher critical fracture energy increase is that the presence of the fibres at the bondline from the ultrathin veil and the associated thickness increase created a blunting effect on the crack tip, and therefore increased the critical energy dissipation values compared to repairs without veil at the bondline.

The incorporation of the polyester veil further increased the critical fracture energy of the DCB repair to 0.562kJ/m$^2$ while a different R-curve pattern was observed revealing that as the crack length was increased indeed more energy was required to continue fracturing the bondline. The noticeable difference was the dramatic increase of the strain energy release rate for the first 10mm of crack growth with the subsequent steady state response thereafter. In this case, the main macroscopic effect responsible for that increase was fibre bridging, which was visible with the naked eye. The high initiation fracture energy was attributed to the very start of the bridging ligament effect and the mechanisms associated with that process. The introduction of both carbon and polyester veils had resulted in an increase in the number of fibres within the bondline. The increase in the number of fibres involved affected the fibre bridging process and resulted in an increase in fracture energy (0.928 kJ/m$^2$), until a plateau value was reached and fibre-bridging saturation occurred.

## 2.4. Failure Mode

The mode-I fracture energy of the DCB repairs studied was closely associated with the relative crack trajectories followed and the failure locus obtained in each type of repair. In general, well-prepared surfaces should produce bonds that after failure exhibit cohesive type of fracture located within the resin/adhesive or within the adherends implying an interlaminar failure mode

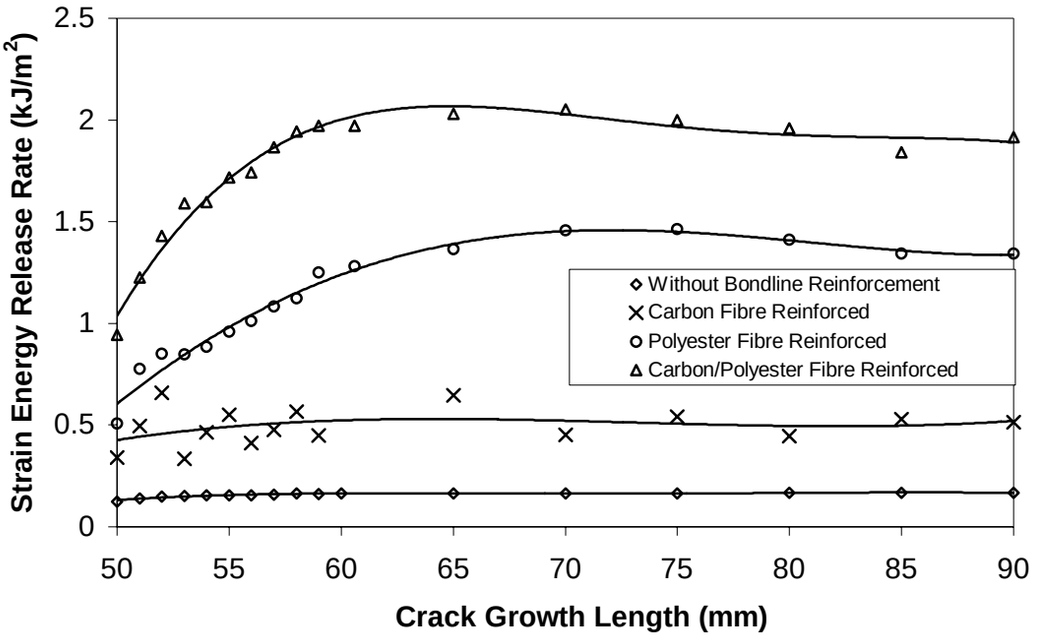


**Fig. 2.** R-curves obtained from the DCB repair testing

.

In the case of repairs without the reinforcing veils at the bondline, certain areas of the parent surface were covered by a thin layer of surface resin; however the dominant failure mode was exposure of fibres suggesting crack propagation close to the surface ply of the parent material. The toughness of the surface resin, as discussed previously, from the Hercules 3501.6 resin system was much lower than the infused LY5052/HY5052 polymerised resin resulting in a preferential fracture path close to the surface fibres. This was verified on the SEM in Fig. 3(a) taken from the fractured specimen where a mixture of fragmented surface fibres and resin is observed.

From the SEM in Fig. 3(b) and Fig. 3(c) it is evident that the incorporation of polyester and carbon veils in the infused bondline region affected the fracture path of the repairs thereby the dissipation of energy. In the case of the DCB repairs reinforced with the carbon veil at the bondline the failure mode showed a cohesive/interfacial fracture area with significant number of broken carbon fibres while both shear hackles as well as brittle cracking from the infused resin were present within the bonded area. A different type of cohesive failure was obtained in the case of DCB repairs reinforced with polyester fibres at the bondline. The crack trajectories followed left behind multiple fibres after significant extension and subsequent plastic deformation from fibre bridging. In the bridging zone, the cracked resin was bridged by intact and/or failed fibres from the polyester veil, which debond, slip and pull out. Fibre fracture occured when and if the bridging stress exceeded the strength of the bridging unit. Therefore, the role of a bridging zone in the fracture resistance of the repairs was of particular importance as the bridging fibres are responsible for inhibiting further crack propagation by carrying a portion of the applied load. This contributed significantly to the resistance of the bondline to further fracture. The damage zone was believed to develop around the crack tip during the early fracture stages, which is difficult to externally observe, and after it reached a steady state (plateau region) propagated in a self-similar manner along with the crack tip. In that case the debond length of the bridging ligaments became longer as the crack opening increased. In addition, more bridging ligaments failed as the crack opening increased.

The combination of the mechanisms that were separately present in the case of carbon and polyester fibre reinforced repairs was observed for the carbon/polyester reinforced repairs. The crack, as discussed in previously was cohesive within the bondline. Magnification of the cohesive region showed significant crack deflection and therefore a non-planar trajectory that hindered propagation as depicted in Fig. 3(a). The crack branched with secondary micro-cracks in different directions, which eventually increased the dissipation of energy.

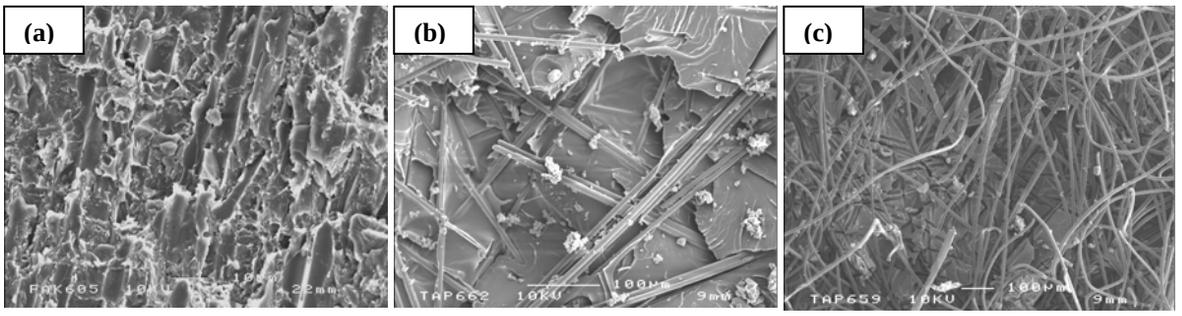


**Fig. 3.** SEM showing characteristic fracture areas of the DCB repairs a) without bondline reinforcement, b) carbon fibre reinforced and c) polyester fibre reinforced

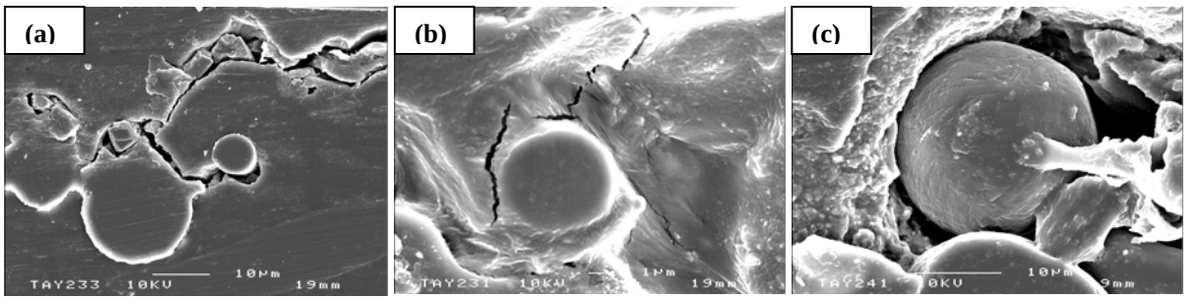


**Fig. 4.** Cross-section of a carbon/polyester fibre reinforced bondline showing the micro-mechanisms affecting the fracture process a) crack deflection at the crack tip, b) resin/adhesive cracking around a well-bonded carbon fibre within the bondline and c) interfacial failure around a poorly-bonded polyester fibre within the bondline

In addition, the crack deflection mechanism involved cracks being impeded by the rigid fibres. This mechanism arose when the crack encountered fibres especially carbon fibres, and became pinned with a tendency to bow out and form secondary cracks perpendicularly to the direction of the crack. The length of the crack front was increased perpendicularly and energy was required to create these new fracture surfaces. Such a process involved the rupture of intrinsic bonds between the infused resin and the bondline fibres (carbon and/or polyester) an implied localized plastic energy dissipation of the resin in the vicinity of the crack.

Rupture of intrinsic bonds is significantly dependent on fibre surface treatment and nature of the fibre. So for instance, the carbon fibres from the carbon veil were shown to exhibit higher interfacial strength with the epoxy resin compared to polyester fibres. That is illustrated qualitatively in Fig. 4(b) and Fig. 4(c) which show individual carbon and polyester fibres respectively past the fracture path of the infused polymerised epoxy resin bondline.

## 3. EVALUATION OF VACUUM INFUSION TOUGHENED REPAIR

### 3.1. Component Preparation and Repair Procedure

The composite aircraft component where the vacuum infusion repair process was assessed consists of a 2.5mm thick carbon skin, manufactured using IM7/8552 prepreg system whilst the sides were blended into a carbon/aluminium honeycomb. In order to test the component in compression, a uniform section of 350x200mm had to be cut out while the top and bottom sides were end-potted using a toughened, unfilled, epoxy matrix so to enable the load to be transferred evenly into the element. The section of interest where the vacuum infusion repair was performed is the carbon skin, which was pre-fabricated according to the following lay-up: $[0°, 0°, 45°, 135°, 0°, 0°, 0°, 45°, 135°, 90°]_s$.

The damage representing a ballistic impact was in the form of a 20mm diameter hole in the centre of the element. The area around the 20mm damage was scarfed manually using a high-speed die-grinder fitted with a 280 grade abrasive pad to a gradient of 1:15. A further 15mm was abraded around the outer perimeter of the scarf in order to remove any surface contamination and therefore to generate suitable bonding surface for the overlap co-infused

ply. A three ply precured carbon patch was bonded to the back face of the panel with a two-part room temperature cure Araldite epoxy adhesive to seal the hole and allow a vacuum to be drawn. The lay-up chosen for the scarf repair patch consisted of ten plies of fabric plus an overlap ply.

The stacking sequence selected was: [(0°/90°), (0°/90°), (+/-45°), (0°/90°), (0°/90°), (0°/90°), (0°/90°), (+/-45°), (0°/90°), (0°/90°), (+/-45°)], where the top over lap ply is the last one in the lay-up sequence. Prior to laying up the fabric a carbon/polyester veil was positioned onto the scarfed recess and extended 15mm passed around its periphery. Then the T300 dry repair plies were assembled over the veil and vacuum infused. The patch during the consolidation and polymerisation process matched perfectly the shape of the scarf recess. Fig. 5 illustrates the design principles of the scarf patch as well as the infusion process while Fig. 6 shows a C-scan of the repaired component indicating the high quality of the manufactured patch.

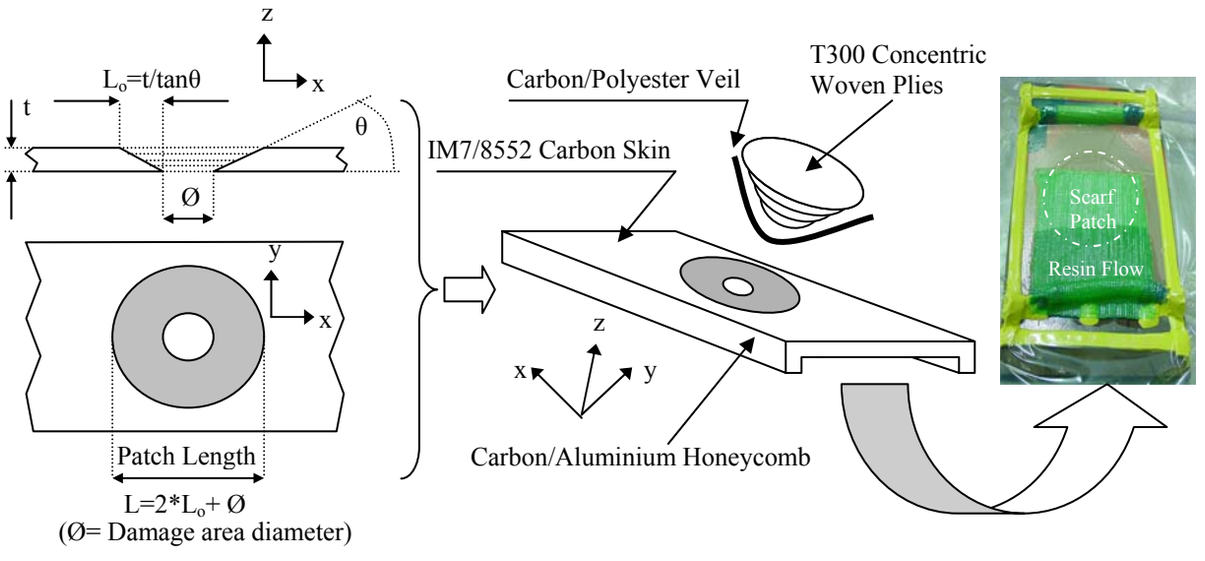


**Fig. 5.** Scarf design and vacuum infusion repair of the component

## 3.2. Testing equipment and monitoring of buckling

The components were tested on a Schenck 1000kN servo hydraulic test machine at a rate of 1mm/min. Strain gauges were attached in the central horizontal axis to study the strain response while two linear variable differential transducers (LVDT) were positioned (one at the centre and one at 35mm distance from the left edge-stiffener) on the back of the components in order to record any out of plane deformations. The Shadow Moiré fringe interferrometry technique was also used to monitor these deformations and identify the buckling response of the components and patch behaviour upon compression. The technique involved initially evenly spraying the front face of the test pieces with a white matt paint. A grating printed on an acetate sheet, with a line spacing of 1line/mm, was held at a uniform distance of 5mm from the surface of the painted test components.

The grating was held by two glass plates and attached to a fixture. Collimated light from a standard slide projector was directed towards the component at an angle of 45º measured from normal to the plane of the component. This produced ‘fringes’ of interference between the grating itself and the shadow caste, by the grating on the surface of the component. These fringes simultaneously served as a datum plane and as an indication of the degree of flexing during testing. Under compressive loading, if the fringes are distorted, they produce interference patterns, which can be considered as deformation contours.

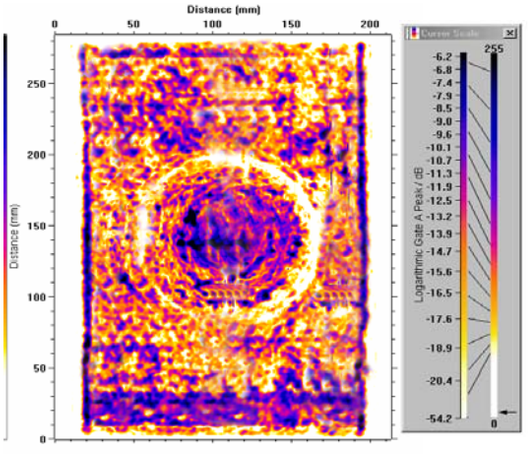


**Fig. 6.** C-scan of the vacuum infused repaired component

### 3.3. Compression Performance of Undamaged and Repaired Components

In general, thin monolithic composite skins are prone to buckling and therefore a repair patch on a composite skin must provide high bond strength and increased bondline toughness in order to prevent the out-of-plane forces (peeling and debonding with subsequent crack formation prior failure) developed upon deformation. Since the compressive behaviour of the carbon skin of the components is dictated by the buckling response, it is interesting first to study the representative Moiré interferograms at different load levels. As shown in Fig. 7 for the undamaged baseline element, fringes started to develop at 20kN near the bottom part indicating that some bending occurred without any specific orientation and shape. At 38kN with a clearly defined bulge at the bottom part a second bulge formed in the middle of the component, which lead to a transition splitting into two well defined bulge configurations at 65kN on the upper part. From that load level onwards it is clear that the compressed component buckled in a wavy pattern, creating three well defined bulges (one and a half wave) up to failure. In that stable post-buckling condition, it was observed that the aspect ratio of the three defined bulges was not similar. This may be associated with the lay up of the carbon skin and the edge honeycomb cell stiffeners judging from the tight confinement of the vertical fringes near the edges of the top and bottom bulges. The interferograms showed that the patch affects the overall mode of deformation relative to the undamaged component. A fringe pattern was defined initially at 20kN around the patch perimeter, signifying that the patch induces an outward deformation. At 39kN three clearly defined bulges were developed with the top one showing the highest fringe density. An increase in the fringe patterns was observed at 65kN and as the load reaches 79kN, which is the load at failure, the middle bulge where the repair patch was located seemed to be suppressed in favour of asymmetric bulging at the top and bottom. A profound asymmetry is observed again in the aspect ratios of the bulges regarding their distribution in both vertical and horizontal axis.

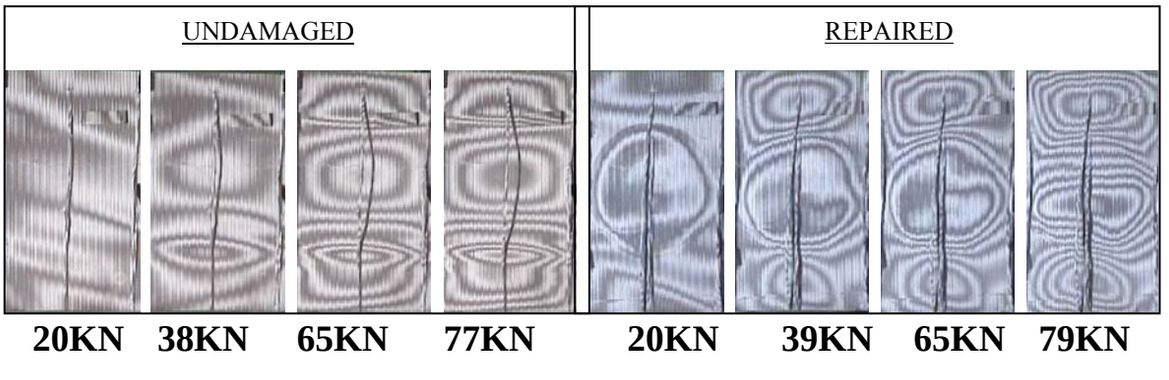


**Fig. 7.** Shadow Moiré deformation fringe sequence of the undamaged and repaired components under axial compression

Fig. 8 compares the traces obtained from the LVDTs positioned in the central area of the components. For the undamaged component, both LVDTs showed a dramatic increase at around 38kN implying that the component buckled at that load level, with LVDT-2 (positioned in the centre) attaining an ultimate value of 3.4mm. It may be assumed that the applied load was shared between the skin and the edge stiffeners, in proportion to their stiffnesses (the product of their respective axial modulus and cross-sectional area). Therefore, the out-of-plane deformation in the middle of the component (carbon skin) is expected to have been higher than at its edges where the stiffeners were located. On the other hand, the patch (especially the co-infused overlap) affected to some extent the global stiffness and therefore the buckling behaviour of the component. The eccentricity of the carbon skin from the patch guarantees that some bending occurred initially, (LVDT reading of around 0.4mm) as the applied displacement was increased. Buckling occurred at 39kN with both LVDT traces having considerably lower values implying resistance to out-of-plane deformation and thus development of significant high peel stresses on the patch. In the region of 70kN the traces showed a sudden unstable jump prior failure.

While failure for the undamaged component resulted from a compressive fracture of the carbon skin leading to skin debonding from the stiffeners with ultimate collapse, the sequence of failure for the repaired component was more complicated. It was observed that the component failed by progressive crack propagation at the upper part of the repair patch from the out-of-plane deformation towards the damage (circular cut-out) and compressive stresses at the edge of the scarf recess. Close to failure it may be assumed that a micro-crack was produced at these high load levels within the bondline, which presumably started propagating when the energy supplied from the applied compressive load reached a critical point equal to the fracture energy of the carbon/polyester veil. Considerable crack arrest would have occurred from the bondline fibres, bridging the crack as suggested by the fluctuation of the traces close to failure preventing a global pop-off. At failure, it was estimated that about 30% of the total patch area had debonded.

For many aircraft primary composite components, the design ultimate loading is the level giving a strain of 4000μstrain (fully factored). This level provides a large safety margin between the likely strains in service (two-thirds of 0.4% strain level) and the material failure strain. The strain gauges attached on the surfaces of the undamaged component recorded compressive strains in excess of the design limit as shown in Fig. 8. Due to buckling the strain gauge traces are not linear although symmetric up to the load level of 45kN.

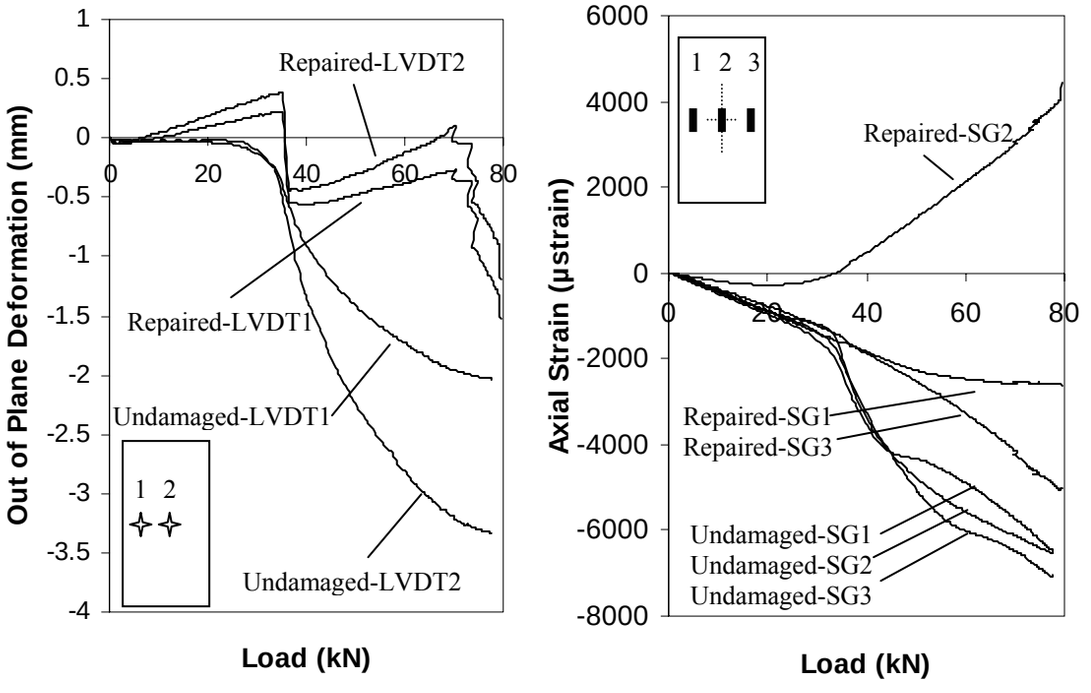


**Figure 8.** Comparison of out of plane deformation-load and axial strain-load traces as obtained from LVDTs and strain gauges positioned on the undamaged and vacuum infusion repaired components

For the vacuum infused repaired component the strain gauges SG1 and SG3 positioned outside the patch area close (25mm) to the edge stiffeners showed compressive strain to failure 2600μstrain and 5000μstrain respectively, implying asymmetric deformation across the width. This comes in agreement with the unevenness observed prior failure of the central bulge of the repaired component as recorded from the Moiré fringes. The strain gauge reading SG2 located on the patch itself revealed considerably lower values up to the critical buckling load due to the local stiffening effect of the infused patch. Thereafter, a dramatic increase, which has been recorded as a tensile strain since the SG2 was located exactly on the buckling crest, attained a strain value of 4537μstrain. If only the strain gauge reading SG2 located on the patch is to be used as the strain level for evaluation of the vacuum infusion repair approach as a potential in-field process, then the ultimate strain value obtained exceeds the critical design limit of 4000μstrain.

## 4. CONCLUSIONS

A novel bondline toughening approach has been developed and tested for vacuum infused repairs. DCB specimens were used to assess the effectiveness of the infused patches by studying the fracture path and calculating the strain energy release rate. For repairs without reinforcing fibres within the bondline the fracture was unstable because the failure locus tended to shift from within the infused resin to the more brittle carbon fibre-to-surface resin interface of the parent laminate. The fracture energy was increased once the failure locus was altered to cohesive from the incorporation of fibres within the bondline in the form of veils and it was shown that this change is dependent on the inherent properties of each veil.
Following the development of the toughening procedure, a composite component taken from an aircraft was repaired by the vacuum infusion repair approach, using a carbon/polyester veil at the bondline. The infused patch has recovered the load-carrying capability of the component, ultimately increasing slightly the failure load. The excess of load that would be carried by the skin around the damage, once the patch was completely interfacially debonded, leading to premature failure, was being carried instead by the well-bonded patch through the carbon/polyester toughened bondline. The bondline reinforcing fibres prevented the crack, initiated from excessive buckling of the component, to entirely peel the patch and so to weaken the strength of the component. The vacuum infused repaired component reached strains on the patched area in excess of the aerospace composite design limit.

## REFERENCES


1. Baker A.A., Repair Techniques for Composite Structures, Composite Materials in Aircraft Structures, D.H. Middleton, Ed.: Longman Scientific and Technical, 207-227, (1990)
2. Russel A.J., Ferguson J.S., Composite Repair Issues on CF-18 Aircraft, AGARD CP 550, Spain, 14/1-14/8, (1994)
3. Baker A.A., Chester R.J., Hugo G.R., Radtke T.C., Scarf Repairs to Graphite/Epoxy Components, Composite Repair of Military Aircraft Structures, AGARD CP 550, Spain, 19/1-19/12, (1994)
4. Soutis C., Duan D.M., Goutas P., Compressive Behaviour of CFRP Laminates Repaired with Adhesively Bonded External Patches, Composite Structures, Vol. 45, 289-301, (1999)
5. Soutis C., Duan D.M., Performance of Composite Repair Patches under Compressive Loading, IMechE Proceedings Int. Conference on Joining and Repair of Plastics and Composites C548/004, 151-160, (1999)
6. Charalambides M.N., Kinloch A.J., Matthews F.L., Adhesively-bonded Repairs to Fibre Composite Materials I: Experimental, Composites Part A, Vol. 29, 1371-1381, (1998)
7. Mahler M., Hahn H.T., Repair Methods for Composite Structures, 8th Japan-US Conference of Composite Materials, Baltimore, 53-62, (1998)
8. Sims G., Bishop G., UK Polymer Composites Sector: Foresight Study and Competitive Analysis, for Department of Trade and Industry, NPL Report MATC (A) 80, (2001)
9. Blackman B., Dear J.P., Kinloch A.J., The Calculation of Adhesive Fracture Energies from Double-Cantilever Beam Test Specimens, Journal of Materials Science Letters, Vol. 10, No. 5, 253-256, (1999)